Journal of Solid State Chemistry 213 (2014) 110–115

Contents lists available at ScienceDirect

Journal of Solid State Chemistry

journal homepage: www.elsevier.com/locate/jssc

High-pressure U_3O_8 with the fluorite-type structure

F.X. Zhang [a,*], M. Lang [a], J.W. Wang [a], W.X. Li [a], K. Sun [b], V. Prakapenka [c], R.C. Ewing [a,b]

[a] Department of Earth and Environmental Sciences, University of Michigan, Ann Arbor, MI 48109, USA
[b] Department of Materials Science and Engineering, University of Michigan, Ann Arbor, MI 48109, USA
[c] Center for Advanced Radiation Sources, University of Chicago, Chicago, IL 60637, USA

ARTICLE INFO

Article history:
Received 7 October 2013
Received in revised form
3 February 2014
Accepted 9 February 2014
Available online 18 February 2014

Keywords:
U_3O_8
Fluorite-type structure
Phase transition
High pressure

ABSTRACT

A new high-pressure phase of U_3O_8, which has a fluorite-type structure, forms at pressures greater than ~8.1 GPa that was confirmed by *in situ* x-ray diffraction (XRD) measurements. The fluorite-type U_3O_8 is stable at pressures at least up to ~40 GPa and temperatures to 1700 K, and quenchable to ambient conditions. Based on the XRD analysis, there is a huge volume collapse (> 20%) for U_3O_8 during the phase transition and the quenched high-pressure phase is 28% denser than the initial orthorhombic phase at ambient conditions. The high-pressure phase has a very low compressibility comparing with the starting orthorhombic phase.

1. Introduction

Due to the unfilled 5*f* shell, uranium has variable covalent bonding states in oxides. The most stable oxidation states are U^{4+} in UO_2 and U^{6+} in UO_3. U^{5+} occurs in some halo complexes [1] and some hyperstoichiometric oxides such as U_2O_5 [2]. U_3O_8 is another stable uranium oxide, the "yellow cake" produced by refining uranium ore, that contains both U^{4+} and U^{6+}. The structure and thermodynamic properties of the most stable UO_2 have been intensively studied [3–9] because of its importance as nuclear fuel. UO_2 has the ideal fluorite structure (AX_2) at ambient conditions. During heating, UO_2 can be oxidized to form non-stoichiometric oxides UO_{2+x} [10,11]. The oxygen stoichiometry of UO_2 can increase continuously to UO_3. There are, however, a number of different phases between UO_2 and UO_3. Previous investigations indicate that uranium oxides (UO_{2+x}) with non-stoichiometric composition can have a fluorite-type structure up to $x < 0.13$ [11]. With further increase of oxygen content, the oxygen atoms become ordered in the lattice and several hyper-stociometric phases will form, such as U_4O_9, U_3O_7, U_2O_5 and U_3O_8 [12–16]. Except UO_2, these higher oxides have multiple polymorphs, some of which are still poorly characterized up to now [17]. From structural, UO_{2+x} with $x < 0.5$ can be regarded as fluorite-related structures though some may have different symmetries. Layered structures will form in UO_{2+x} when $x > 0.5$, such as α-U_3O_8 [16–18]. The structural investigation of the higher uranium oxides under a variety of extreme environments is important because these phases may be formed at the different stages of the nuclear fuel cycles (high temperature and pressure).

As an external parameter, pressure has a significant effect on the structure and physical properties of materials causing phase transitions [19,20], disordering [21,22], metal-insulator transition [23,24] or even a superconducting transition [25]. Some high-pressure phases, such as diamond can persist at ambient conditions as metastable phases. However, most high-pressure phases are not stable when pressure is released. Actinide elements have unfilled *f* electron shells with lower ionization energies. Except for UO_2, the bonding states of actinides and structural behavior of actinide compounds under extreme pressure/temperature conditions are not well studied. Previous experiments [5–7] demonstrated that the isometric UO_2 is not stable and transformed to a cotunnite-type structure at pressures above 34 GPa [7]. The critical pressure is significantly lower at elevated temperatures. The high-pressure cotunnite phase of UO_2 has a very different bond environment, which may lead to interesting physical properties. Unfortunately, the high-pressure phase of UO_2 is not quenchable [5–7]. There are only a few reports on the structural behavior of higher oxides UO_3 at high pressure conditions with very limited data quality [26,27]. The same applies to the hyperstoichimetric UO_{2+x} compositions at high pressure. Six polymorphs of U_3O_8 have been reported [17], but not all of them are well characterized. At ambient conditions, the layered α-U_3O_8 is a pseudo-hexagonal structure (orthorhombic) and it transforms to a real hexagonal structure (with space group of *P*-62*m*) at elevated temperature (~350 °C) [28]. At temperatures

* Corresponding author.
E-mail address: zhangfx@umich.edu (F.X. Zhang).

http://dx.doi.org/10.1016/j.jssc.2014.02.012
0022-4596

higher than 875 °C, the structure of U_3O_8 changes continuously, but it may be related to the loss of oxygen content [28]. In this study, we describe the structure of α-U_3O_8 at high pressure and high temperature using *in situ* synchrotron XRD analysis.

2. Experimental

The U_3O_8 was synthesized by reduction of a UO_3 powder (International Bio-Analytical Industries, Ltd.) at 200 °C for 11 h in a flowing gas (Ar/H_2, 98/2) atmosphere. The oxidation status of U was determined with x-ray photoelectron spectroscopy (XPS) at Kratos Axis Ultra XPS facility in a very high vacuum ($<10^{-9}$ Torr) environment. High pressure was generated by using a symmetric diamond anvil cell with 300 μm culet diamond anvils. Hardened stainless steel and rhenium gaskets were used for room temperature and high temperature measurements, respectively. The *in situ* XRD measurements were carried out at GSECARS, Advanced Photon Source, Argonne National Laboratory [29]. The mixture of methanol/ethanol (4/1 volume) served as the pressure medium for room temperature experiments and no medium was used for the laser heating experiments. Fluorescence from ruby chips was used as a pressure standard [30] for room temperature measurements and Au was used as a pressure marker in the laser heating experiments. The x-ray wavelength was 0.4066 Å and 0.3344 Å for room temperature and high temperature experiments, respectively. Debye rings were recorded with CCD x-ray detectors and the two- dimensional XRD profiles were integrated by using the Fit2D software [31]. Powder CeO_2 or LaB_6 was used as an external standard to calibrate the instrumental parameters. The obtained XRD patterns were refined by the Rietveld method using the program Fullprof [32].

XRD measurements with a laboratory XRD facility confirmed that the fabricated sample was nearly a single phase of α-U_3O_8. A schematic structure of the layered α-U_3O_8 is shown in Fig. 1a. The U atoms are 7-fold coordinated with oxygen, of which five are on the same plane and the other two oxygen atoms are on each side of the plane forming a pentagon-based bi-pyramid. The refined unit cell parameters of α-U_3O_8 are $a=6.751(1)$ Å, $b=11.978(2)$ Å and $c=4.1607(8)$ Å in space group *C2mm* (Fig. 1b). The lattice parameters are consistent to previously published data [16] and the structural details are listed in Table 1. For XPS measurements, UO_2 and UO_3 were used as energy and composition calibration standards. The XPS spectrum of U_3O_8 confirmed the mixed covalent states of U^{4+} and U^{6+} in the synthesized sample. XPS spectra are usually sensitive to the oxidation states of ions and their bonding environment in the structure of material. In the present measurements, the binding energies of $4f_{5/2}$ and $4f_{7/2}$ electrons for U^{4+} in UO_2 are 381.3 eV and 392.3 eV, respectively. The corresponding energies for U^{6+} in UO_3 are 382.2 eV and 393.0 eV. The measured U 4*f* binding energy in U_3O_8 contains obviously two peaks (Fig. 1c). Based on the UO_2 and UO_3 standards, the composition of the synthetic U_3O_8 determined from the measured XPS spectrum is $UO_{2.8}$. The oxygen content is slightly higher than the nominal value of 2.67, which may be due to absorbed oxygen on the surface of the powder sample during sample handling.

The evolution of XRD patterns of U_3O_8 at high pressure and room temperature is shown in Fig. 2a. A phase transition is clearly observable initially at a pressure of about 8.1 GPa. The phase transition is very sluggish, processing over a pressure range of 6.3 GPa to more than 20 GPa. The strongest diffraction peak (1 3 0) from the original α-U_3O_8 phase near 7° 2θ, is still evident at 22.5 GPa. Above that pressure, the XRD patterns suggest a simple fluorite-type structure for the high-pressure phase, which persists up to the maximum pressure of ~40 GPa in this work. Importantly, this fluorite-type structure is quenchable at ambient conditions. UO_{2+x} has a fluorite-type topology up to $x<0.5$. However, when $x>0.25$, the structure becomes tetragonal [15] or even monoclinic [16]. The XRD patterns of U_3O_8 at 13.5 GPa and 16.1 GPa clearly show additional diffraction peak(s) around the strongest (1 1 1) diffraction maximum of the fluorite structure.

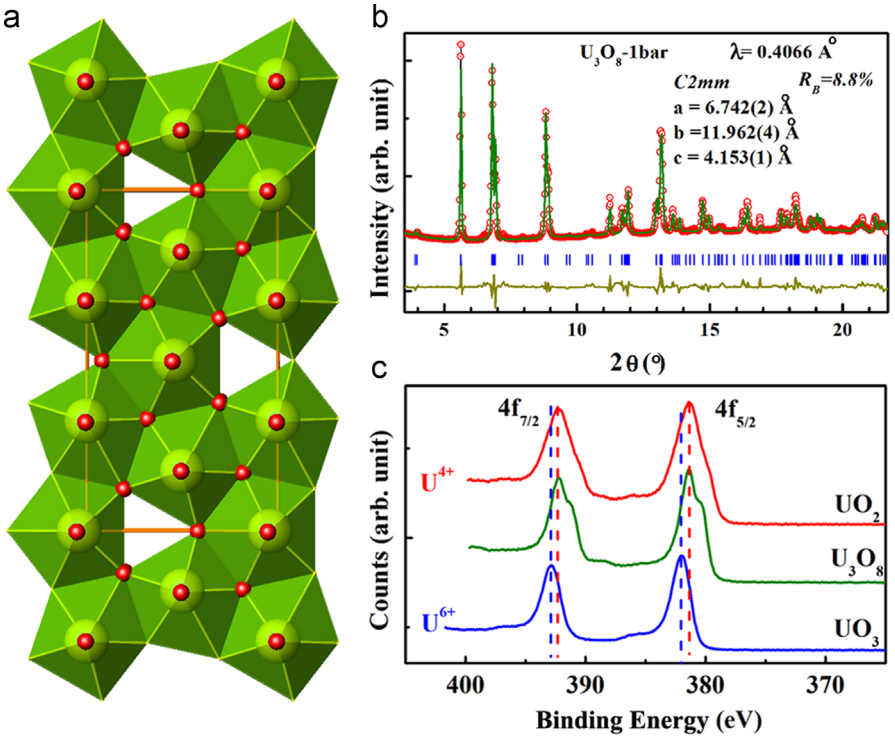

Fig. 1. (a) Schematic crystal structure of α-U_3O_8; (b) XRD profile of U_3O_8 at ambient conditions refined with the orthorhombic α-U_3O_8 structure model; (c) The U_{4f} XPS spectra of UO_2, U_3O_8 and UO_3.

Table 1
The atomic position and occupancies of the starting orthorhombic phase U_3O_8 and quenched sample after laser heating at 38 GPa refined from the XRD patterns.

Orthorhombic phase[a] (*C*2*mm*) a=6.751(1) Å, b=11.978(2) Å, c=4.1607(8) Å						Cubic phase[a] (*Fm*-3*m*) a=5.415(1) Å					
Atom	Site	*x*/*a*	*y*/*b*	*z*/*c*	Occ.	Atom	Site	*x*/*a*	*y*/*b*	*z*/*c*	Occ.
U1	2*a*	0.963(3)	0	0	1	U	4*a*	0	0	0	0.88(2)
U2	4*d*	0	0.325(1)	0	1	O1	32*f*	0.259	0.259	0.259	1/4
O1	2*a*	0.582	0	0	1	O2	48*i*	0.5	0.644	0.644	0.033(7)
O2	2*b*	0.95	0	1/2	1						
O3	4*d*	0.194	0.1239	0	1						
O4	4*d*	0.317	0.3294	0	1						
O5	4*e*	0.996	0.3218	½	1						

[a] The oxygen positions in the orthorhombic phase are not refined.

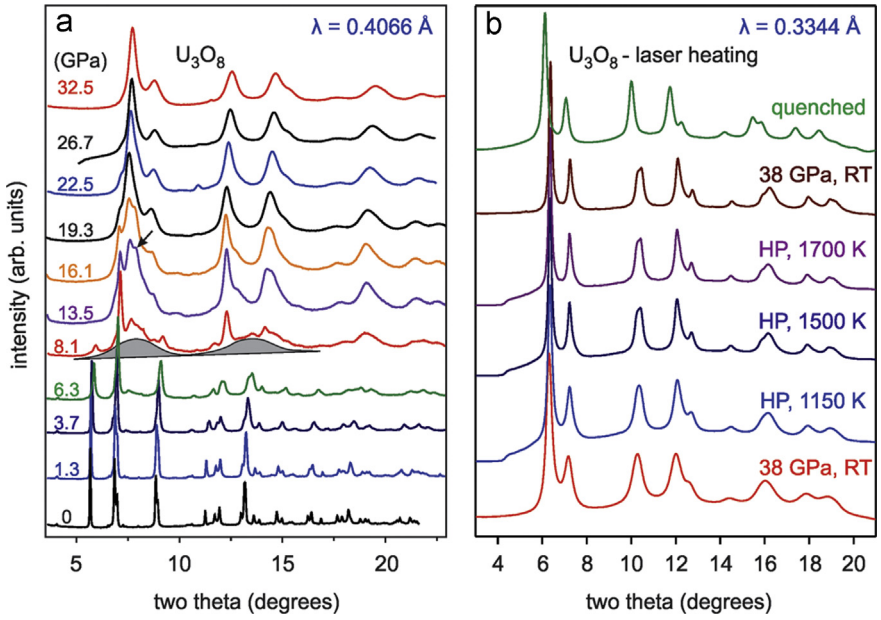

Fig. 2. (a) XRD patterns of U_3O_8 measured at high pressure and room temperature. The α-U_3O_8 starts to transform to the fluorite-type structure at 8.1 GPa. Note the diffuse scattering as evidence for the formation of amorphous domains; (b) XRD patterns of the fluorite-type high-pressure phase of U_3O_8 at high-pressure and high-temperature. The fluorite-type structure is stable during heating and quenchable. There is no significant change of the unit cell parameter, which evident that there is no obvious oxygen release during the process.

This suggests that the high-pressure phase is not an ideal cubic structure at the beginning of the phase transition, but has a lower symmetry. The refinement results indicate that the unit cell of the fluorite-type U_3O_8 deviates slightly from cubic at high pressures. The maximum deviation of the (2 0 0) plane of the high-pressure phase at 32 GPa is ~1.4% from the ideal value.

Due to the extra oxygen atoms in the lattice, the structure of the high-pressure phase cannot be the ideal fluorite structure. Thus, a modified fluorite-structure model [33] was used to refine the XRD patterns. In this model, the position of oxygen atoms deviates from the 8*c* site in ideal fluorite to a 32*f* site with additional small amount of oxygen occupying a 48*i* site and another 32*f* site in the lattice. Rietveld refinement suggests that the first 32*f* site is fully occupied and the second 32*f* site is nearly empty (<0.001). The 32*f* site in the structure model is just a deviation from the ideal position of 8*c* in fluorite structure and the maximum possible occupancy is 0.25. During refinement, the fractional occupancy of O at 32*f* site is actually fixed at 1/4. Due to the big difference of x-ray scattering ability between the heavy element U and the light element O, it is impossible to get reliable values for the coordinates of O from the XRD refinement. All the atomic coordinates of O atoms are not refined. Refinement results suggest that only a small amount of oxygen atoms are located on the 48*f* site around the uranium atom in the center of the unit cell. In addition, the U site (4*a*) is not fully occupied. Because the 48*f* and the second 32*f* sites are quite close to U at the 4*a* site (~2.09 Å), it is reasonable to assume that the occupancy at these sites is very low. Fig. 3a and b shows the 32*f* and 48*i* oxygen sites in the fluorite-related structure, respectively. The 32*f* site is around the 8*c* site in ideal fluorite structure. The 12 48*i* sites form cages in the unit cell and one cage is at the center of the unit cell (Fig. 3b). Due to the low occupancy, the statistical occupancy of the 12 oxygen atoms at the 48*i* sites around one U atom is 0.39(9). The structural details of the quenched high-pressure phase based on Rietveld refinement are summarized in Table 1.

The phase relations between U_3O_8 and UO_2 have been discussed previously [10]. The phase transformation from UO_2 with the ideal fluorite-structure to the layered α-U_3O_8 structure was explained to occur by the displacement of the (1 1 1) planes in UO_2 structure. This mechanism may not apply for the transformation from layered U_3O_8 to a fluorite-type structure at high pressures. At the onset of transformation at 8.1 GPa (Fig. 1a), diffused scattering in the XRD pattern indicates the formation of disordered phase. However, we cannot characterize the existence of the amorphous phase by XRD method. With further increase of pressure, the diffraction maxima (1 1 1) and (2 0 0), from the fluorite structure increase their intensities gradually. Due to the non-stiochiometric oxygen in the structure, the fluorite-type high-pressure phase

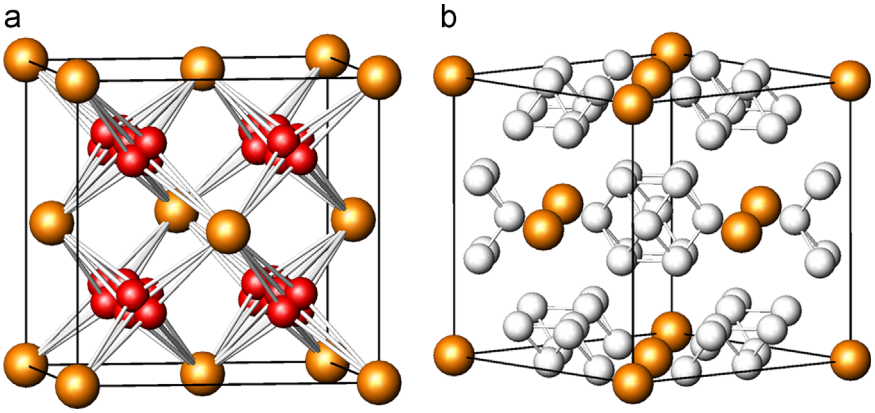

Fig. 3. Schematic structure of the fluorite-type high-pressure phase (a) O1 atoms at 32*f* sites are surrounding the 8*c* site in ideal fluorite structure; (b) 12 of O2 at 48*f* form a cage around the center of the unit cell, and the total oxygen occupancy for the 12 O2 sites is approximately 0.39. The spheres in golden, red and white colors represent U at 4*a* site and O at 32*f* and 48*i* sites, respectively. (For interpretation of the references to color in this figure legend, the reader is referred to the web version of this article.)

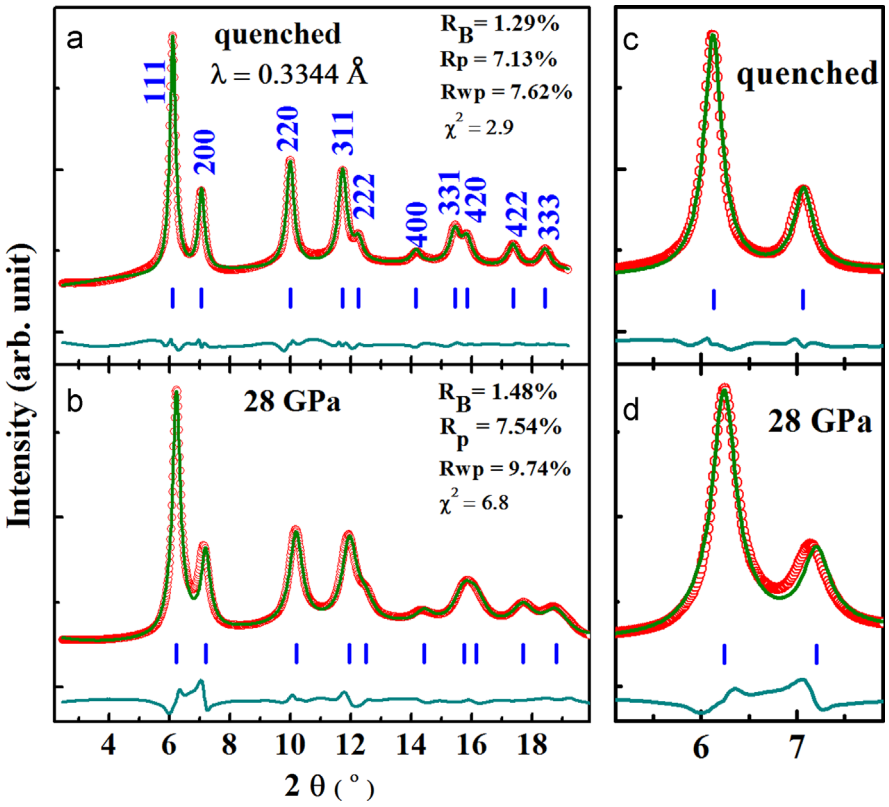

Fig. 4. The Rietveld refinement results of XRD patterns of U_3O_8 with the fluorite-type structure model for the quenched sample ((a), (c)) and at 28 GPa ((b), (d)). The quenched sample has perfect cubic symmetry.

must contain a lot of structural defects. This may limit the growth to large-sized grains, and explains why the fluorite-type high-pressure phase has distinctively broad diffraction peaks.

In order to study the phase stability of the new actinide oxide phase at extreme conditions, α-U_3O_8 sample was pressurized in another run to 38 GPa without a pressure medium and subsequently laser heated to high temperatures up to 1700 K. Fig. 2b shows the XRD patterns of the high-pressure phase during heating at various temperatures. The *in-situ* XRD patterns clearly indicated that the fluorite-type high-pressure phase of U_3O_8 has no obvious change during heating at high pressures. The fluorite-type structure after laser heating is also quenchable to ambient conditions. Fig. 4 shows the fitting results of the high-pressure phase refined with a fluorite structure model at ambient conditions and 28 GPa, respectively. The pattern at 28 GPa shows a small deviation from the cubic model. The enlarged two theta region around (2 0 0) peak (Fig. 4d) shows that the fitting with cubic fluorite model is not perfect. However, the deviation is very small. The maximum deviation at 28 GPa from the ideal cubic structure is the (2 0 0) peak (0.8%) and the quenched sample can be well described as a cubic structural model without apparent deviation in the resolution limit of the instrument. For simplicity, we only use the cubic structural model to estimate the unit cell volume in the whole pressure range. The pronounced peak broadening in the XRD profiles of the high-pressure phase are not caused by strain or stress in the sample because such a strain would be annealed during heating, but the laser heated sample still had very broad peaks. The broad peak width in the high-pressure phase is due to the small size of the crystallites. The estimated grain size of the sample before and after laser heating, based on Scherer's formula and Williamson-Hall plot is 14.1 nm and 18.1 nm, respectively. The

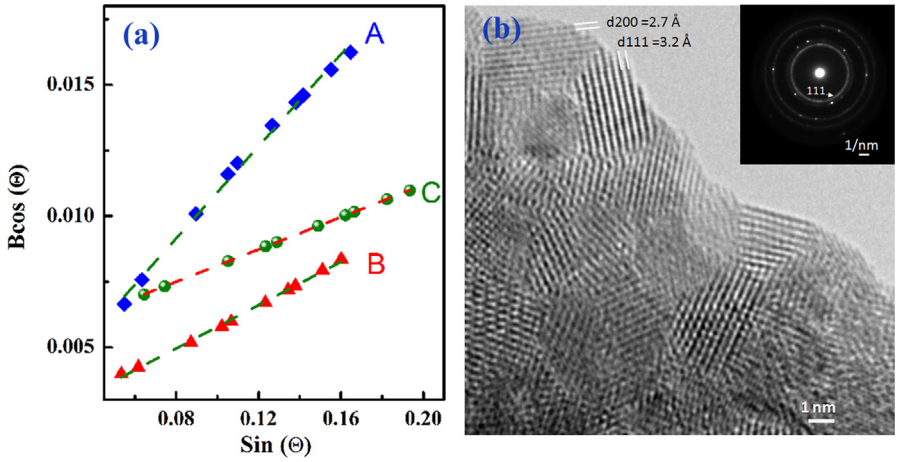

Fig. 5. (a) Williamson-Hall Plot for the quenched U_3O_8 samples, A: Sample at 37.5 GPa and room temperature measured with x-ray wavelength of 0.3344 Å, grain size 14.1 nm; B: sample A with laser heated and quenched from high pressure/temperature to ambient conditions, grain size: 18.1 nm; C: Sample quenched from 32 GPa and room temperature with methanol/ethanol medium and measured with x-ray wavelength of 0.4066 Å, grain size: 7.3 nm (b) TEM image of the quenched sample (c) from high pressure and room temperature.

estimated grain size by XRD of the quenched sample with *M*/*E* pressure medium is 7.3 nm, which is consistent with high resolution TEM observations (Fig. 5).

During heating, we did not observe any unusual change in the unit cell parameters except for the sharpening of the individual peaks and the thermal expansion for the fluorite-type high-pressure phase, which suggests that there is no detectable change of oxygen content. Previous experiments suggest that the unit cell of fluorite-type UO_{2+x} shrinks when extra oxygen atoms exist in the structure and the unit cell parameter for UO_{2+x} follows the empirical formula [34]: $a=5.4696-0.1495x$. This equation is only applicable for $x<0.25$ because UO_{2+x} has different structures when $x>0.25$. The high-pressure phase of U_3O_8 has a much larger x ($\sim$0.8) and the unit cell parameter may not follow the equation though it has a fluorite-type structure. The measured unit cell parameter of the fluorite-type U_3O_8 after laser heating at ambient conditions is 5.415 (1) Å, which is much smaller than that of UO_2 (5.4682 Å [35]).

The extra oxygen in the fluorite-type structure greatly enhanced its structural stability. For stoichiometric UO_2, both experimental and theoretical investigations [7] suggest that the fluorite structure transformed to a cotunnite high-pressure structure at pressures greater than 34 GPa. The critical transition pressure can be lowered to less than 20 GPa with heating. For U_3O_8, the high-pressure fluorite-type structure is stable up to $\sim$40 GPa, even heated to 1700 K. In the fluorite-type high-pressure phase, most of the oxygen atoms occupy the 32*f* (*x*, *x*, *x*) site, not the 8*b* site (1/4,1/4,1/4). The coordinate *x* is variable, and O atoms thus have more freedom to adjust in accordance to the change of external pressure and temperature.

Pressure dependence of the unit cell (per formula of UO_{2+x}) is shown in Fig. 6 and the corresponding data are listed in Table 2. The volume change of α-U_3O_8 at high pressure is distinct. The two polymorphs of U_3O_8 have very different compressibility. The fit of the *P*–*V* curves with the Birch–Murnaghan equation of state yields a bulk modulus of 78(2) GPa for α-U_3O_8 and 375(47) GPa for the high-pressure phase, respectively, when the pressure derivative is fixed at 4. The α-U_3O_8 is a very soft material and the bulk modulus is comparable to that of metal Al (76 GPa [36]), while the high-pressure fluorite-type structure is difficult to be compressed. The bulk modulus of the fluorite-type high-pressure phase is greater than that of UO_2 (207 GPa [7], 166 GPa [5]). This is reasonable because there are more oxygen atoms in the unit cell of U_3O_8, which has an even smaller volume than that of UO_2. U_3O_8 has a huge volume collapse ($>$22%) during the phase transition from

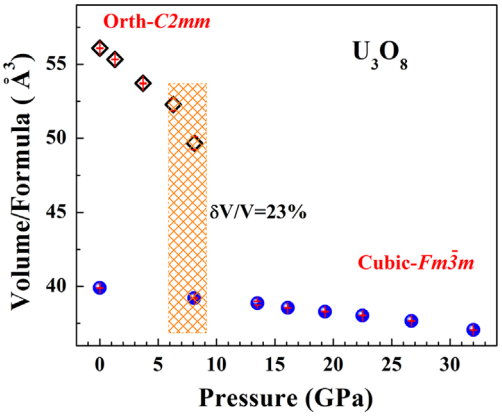

Fig. 6. Pressure dependence of the unit cell volume of U_3O_8 (per formula of $U_{1-\delta}O_{2+x}$).

the orthorhombic phase to the fluorite-type cubic phase. The quenched high-pressure phase is 28% denser than the starting material. The huge volume collapse is related to the structure of α-U_3O_8 and transition mechanism. α-U_3O_8 has a pseudo-hexagonal symmetry, but it is not a close-packed structure, because U atoms in the neighboring layers are exactly on the top and bottom of the U atoms in the middle layer. The fluorite-type cubic phase is a close-packed structure and it is not difficult to understand the huge volume collapse during the phase transition. The U sublattice in different layers shifts during the phase transition at high pressures. Some of the U–O bonds may break during the phase transition. It is reasonable to assume that oxygen may lose during the phase transition. Early heating experiments have revealed that U_3O_8 lost partial oxygen when the temperature is higher than 875 °C [28]. However, we did not observe any oxygen loss from the analysis of the observed XRD patterns and the lattice constants. We noticed that Lipp et al. [37] have measured the Raman spectrum of U_3O_8 till to 44 GPa with Ne pressure medium and they observed a similar phase transition. But they did not observe any detectable molecular oxygen during pressurization. We used *M*/*E* pressure medium for XRD experiments and no medium for laser heating experiments. The similar results suggest that the pressure-induced phase transition in α-U_3O_8 is intrinsic and not related to the pressure transmitting medium.

Table 2
Unit cell parameters of U_3O_8 at various pressures.

GPa	Orthorhombic low-pressure phase (*C*2*mm*) *a*(Å), *b*(Å), *c*(Å), *V*(Å^3)	Cubic phase (*Fm*-3*m*) *a*(Å), *V*(Å^3)	Unit cell volume (Å^3) per UO_{2+x}[a]
0	6.751(1), 11.978(2), 4.1607(8), 336.5(1)		56.0(1)
1.3	6.7369(9), 11.907(2), 4.1382 (6), 331.94((8)		55.3(1)
3.7	6.721 (3), 11.740(4), 4.084 (1), 322.3 (2)		53.7(1)
6.3	6.70 (4), 11.62(6), 4.027(2), 314(2)		52.3(4)
8.1	6.57(5),11.40(9), 3.979(3), 298(3)	5.392(4), 156.8(2)	49.7(5), 39.2(1)
13.5		5.377(1), 155.47((7)	38.9(1)
16.1		5.362(1), 154.18(6)	38.5(1)
19.3		5.350(1), 153.16(6)	38.3(1)
22.5		5.338(1), 152.12(6)	38.0(1)
26.7		5.321(1), 150.66(6)	37.7(1)
32.0		5.292(1), 148.23(6)	37.1(1)
0[b]		5.424(1), 159.57(6)	39.9(1)

[a] For simplicity, unit cell volume is used here and the actual chemical content is $U_{1-\delta}O_{2+x}$.
[b] Quenched to ambient conditions.

In summary, a dense fluorite-type form of U_3O_8 was synthesized by pressurizing α-U_3O_8. Formation commenced at just more than 8 GPa. The phase transition occurs over a broad range from 6.3 GPa to 22.5 GPa. The high-pressure phase has a very low compressibility. The quenched high-pressure phase is 28% denser than the starting U_3O_8 at ambient conditions and we did not find any observable oxygen loss during the phase transition.

Acknowledgment

This work was supported as part of the Materials Science of Actinides, an Energy Frontier Research Center, funded by the Office of Basic Energy Sciences under Award Number DE-SC0001089. The XRD measurement at GSECARS, Advanced Photon Source (APS), Argonne National Laboratory is supported by the National Science Foundation - Earth Sciences (EAR-0622171), Department of Energy - Geosciences (DE-FG02-94ER14466) and the State of Illinois. Use of the Advanced Photon Source was supported by the U. S. Department of Energy, Office of Science, Office of Basic Energy Sciences, under Contract no. DE-AC02-06CH11357.

References

[1] J. Selbin, Chem. Rev. 69 (1969) 657.
[2] R.E. Rundle, N.C. Baenziger, A.S. Wilson, R.A. McDonald, J. Am. Chem. Soc. 70 (1948) 99.
[3] D. Labroche, O. Dugne, C. Chatillon, J. Nucl. Mater. 312 (2003) 50.
[4] B.T.M. Willis, J. Phys 25 (1964) 431.
[5] S. Greaux, L. Gautron, D. Andrault, N. Bolfan-Casanova, N. Guignot, J. Haines, Am. Mineral. 93 (2008) 1090.
[6] H.Y. Geng, Y. Chen, Y. Kaneta, M. Kinoshita, Phys. Rev. B: Condens. Matter 75 (2007) 054111.
[7] M. Idiri, T. Le Bihan, S. Heathman, J. Rebizant, Phys. Rev. B: Condens. Matter 70 (2004) 014113.
[8] J.W. Wang, R.C. Ewing, U. Becker, Phys. Rev. B: Condens. Matter 88 (2013) 024109.
[9] J.F. Marin, P. Contamin, J. Nucl. Mater. 30 (1969) 16.
[10] G.C. Allen, N.R. Holmes, J. Nucl. Mater. 223 (1995) 231.
[11] R.J. McEachern, P. Taylor, J. Nucl. Mater. 254 (1998) 87.
[12] B. Gelbeoch, C. Piekarski, P. Perio, Acta Crystallogr. 14 (1961) 837.
[13] N. Masaki, K. Doi, Acta Crystallogr., Sect. B: Struct. Sci 28 (1972) 785.
[14] J.P. Lauriat, G. chevrier, J.X. Boucherle, J. Solid State Chem. 80 (1989) 80.
[15] D.J.M. Bevan, I.E. Grey, B.T.M. Willis, J. Solid State Chem. 61 (1986) 1.
[16] B.O. Loopstra, Acta Crystallogr. 17 (1964) 651.
[17] R. Herak, B. Jovanovic, Inorg. Nucl. Chem. Lett. 5 (1969) 693.
[18] B.O. Loopstra, Acta Crystallogr., Sect. B: Struct. Sci 26 (1970) 656.
[19] A.R. Oganov, R. Martonak, A. Laio, P. Raiteri, M. Parrinello, Nature 438 (2005) 1142.
[20] F.X. Zhang, J.W. Wang, J. Lian, M. Lang, U. Becker, R.C. Ewing, Phys. Rev. Lett. 100 (2008) 045503.
[21] F.X. Zhang, M. Lang, Z. Liu, R.C. Ewing, Phys. Rev. Lett. 105 (2010) 015503.
[22] F.X. Zhang, B. Manoun, S.K. Saxena, C.S. Zha, Appl. Phys. Lett. 86 (2005) 181906.
[23] H. Okabe, N. Takeshita, M. Isobe, E. Takayama-Muromachi, T. Muranaka, J. Akimitsu, Phys. Rev. B: Condens. Matter. 84 (2011) 115127.
[24] V. Pardo, W.E. Pickett, Phys. Rev. B: Condens. Matter 85 (2012) 045111.
[25] A.F. Kusmart, B. Sipos, H. Berger, L. Forro, E. Tutis, Phys. Rev. Lett. 103 (2009) 236401.
[26] T.I Dyuzheva, N.A. bendeliani, V.V. Brazhkin, L.M. Kuznetshov, J. Alloys Compd. 315 (2001) 59.
[27] S. Siegel, H. Hoekstra, E. Sherry, Acta Crystallogr. 20 (1966) 292.
[28] R.J. Ackermann, A.T. Chang, J. Inorg. Nucl. Chem. 39 (1976) 75.
[29] V.B. Prakapenka, A. Kubo, A. Kuznetsov, A. Laskin, O. Shkurikhin, P. Dera, M. L. Rivers, S.R. Sutton, High Pressure Res. 28 (2008) 225.
[30] H.K. Mao, J. Xu, P.M. Bell, J. Geophys. Res. 91 (1986) 4673.
[31] A. Hammersley, Computer Program Fit 2d, ESRF, Grenoble, 1998.
[32] T. Roisnel, J. Rodriguez-Carvajal, Mat. Sci. Forum, in: Proceedings of Seventh Eur. Powder Diffr. Conf. (EPDIC7), 118 (2000).
[33] B.T.M. Willis, Nature 197 (1963) 755.
[34] V.A. Alekseyev, L.A. Anya'yeva, R.P. Rafal'skiy, Intern. Geol. Rev. 23 (1979) 1229.
[35] S.A. Barrett, A.J. Jacobson, B.C. Tofield, B.E.F. Fender, Acta Crystallogr., Sect. B: Struct. Sci 38 (1982) 2775.
[36] A.M. James, M.P. Lord, Macmillan's Chemical and Physical Data, MacMillan, London, UK, 1992.
[37] M.J. Lipp, Z.S. Jenei, J. Park Klepeis, W.J. Evans, Lawrence Livermore National Laboratory Report, LLNL-TR-522251 (2011).